Applied Surface Science 319 (2014) 189–196

Contents lists available at ScienceDirect

Applied Surface Science

journal homepage: www.elsevier.com/locate/apsusc

Effect of calcination temperature on physical parameters and photocatalytic activity of mesoporous titania spheres using chitosan/poly(vinyl alcohol) hydrogel beads as a template

R. Jiang[a,b,c], H.-Y. Zhu[a,b,*], H.-H. Chen[c], J. Yao[a,b], Y.-Q. Fu[b], Z.-Y. Zhang[a], Y.-M. Xu[c,**]

[a] Department of Environmental Engineering, Taizhou University, Taizhou 318000, PR China
[b] Zhejiang Provincial Key Laboratory of Plant Evolutionary Ecology and Conservation, College of Life Science, Taizhou University, Taizhou 318000, PR China
[c] State Laboratory of Silica Materials and Department of Chemistry, Zhejiang University, Hangzhou 310027, PR China

ARTICLE INFO

Article history:
Received 12 May 2014
Received in revised form 30 June 2014
Accepted 30 June 2014
Available online 7 July 2014

Keywords:
Mesoporous titania
Phenol
Photocatalytic activity
Chitosan
Poly(vinyl alcohol)
Calcination temperature

ABSTRACT

Mesoporous titania spheres were prepared by modified sol–gel method using chitosan/poly(vinyl alcohol) hydrogel beads as a template. Effects of calcination temperature on physical parameters were investigated by X-ray diffraction (XRD), N_2 adsorption–desorption, Fourier transform infrared (FT-IR) spectra, thermogravimetry and differential thermal analyses (TG-DTA), high-resolution transmission electron microscope (HRTEM) and scanning electron microscopy (SEM). The photocatalytic activity of mesoporous titania spheres prepared was also evaluated by photocatalytic degradation of phenol as a model molecule under UV irradiation. With increasing calcination temperature, average crystallite size and pore size increased. In contrast, Brunauer–Emmett–Teller (BET) specific surface areas, porosity and pore volumes steadily decreased. Results of characterization proved that prepared titania spheres with highly organized pores were mesoporous structure. The photocatalytic activity of mesoporous titania spheres calcined at 500 °C was more effective than those calcined at other temperatures, which were attributed to the porous structure, large BET surface area, crystalline, and smaller crystallite size. This work may provide new insights into the preparation of novel mesoporous titania spheres and further practical applications in the treatment of wastewater.

1. Introduction

To solve increasingly serious problems of water pollution, various novel materials are being applied in the field of environmental pollution control [1–4]. Among all kinds of materials, titanium oxide (TiO_2) is an extremely interesting semi-conductor material due to its excellent properties such as high photocatalytic activity, low cost, environmental friendliness and chemical stability [2,5]. It is well known that effectiveness of titania as a photocatalyst is very sensitive to its crystal phase, particle size, surface area and crystallinity [6–8]. Recently, many research attentions have been focused on the fabrication of mesoporous TiO_2 with high BET surface area and photocatalytic activity [7–11]. Mesoporous titania materials have been reported for applications in photocatalysis, adsorption, separation, etc. [9,11–14]. However, practical use of such mesoporous titania materials in nano grade presents some drawbacks, such as agglomeration during utility and difficulty in separating and reclaiming them from treated effluent [15].

To overcome above drawbacks, the development of mesoporous TiO_2 microspheres supported in porous frameworks such as structured silica and alumina (Al_2O_3) became a good alternative to extra beneficial properties due to synergistic effects with the porous matrix [16–19]. Additionally, those mesoporous TiO_2 materials obtained by such synthesis method have been defined particle size and suitable mean pore size [19]. However, it is difficult to remove those porous frameworks used in the preparation of mesoporous TiO_2 materials. Chitosan (CS), (1,4)-2-amino-2-deoxy-D-glucosamine, is a natural basic, hydrophilic, nontoxic and biocompatible biopolymer obtained by the alkaline deacetylation of chitin [20]. Moreover, chitosan has good chelating ability with transition metal ions, which makes it possible for its metal ion complexes to be used as precursors to synthesize nanoparticles [3,21–23]. All the above-mentioned properties also make chitosan a very good candidate to design all kinds of functional materials [21,23]. Previous study has revealed that chitosan

* Corresponding author at: No. 1139 Avenue, Jiaojiang District, Taizhou, Zhejiang Province 318000, PR China. Tel.: +86 139 8967 2070; fax: +86 576 8866 0338.
** Corresponding author. Tel.: +86 571 87952410; fax: +86 571 87951895.
E-mail addresses: zhuhuayue@126.com (H.-Y. Zhu), xuym@css.zju.edu.cn (Y.-M. Xu).

http://dx.doi.org/10.1016/j.apsusc.2014.06.185
0169-4332/

exhibited a multifunctional performance with TiO_2 in heterogeneous photocatalysis technology by enhancing adsorption-photocatalysis [23]. As distinctive intermolecular interactions and formation of hydrogen bonds between poly(vinyl alcohol) (PVA) and chitosan, chitosan/PVA composite has good mechanical property, unique three-dimensional structure, favorable film- and particle-forming property and adjustable pore size, which allows considering chitosan/PVA hydrogel beads as ideal adsorbents for removal of metal ions and organic dye from aqueous solutions [24–29]. Therefore, it also becomes possible that chitosan/PVA hydrogel beads will be used as an alternative template to prepare mesoporous materials. However, to the best of our knowledge, study on the effect of calcination temperature on physical parameters and photocatalytic activity of mesoporous titania microspheres using chitosan/PVA hydrogel beads as a template has not yet been studied.

In this study, mesoporous titania spheres were prepared using chitosan/PVA hydrogel beads as a template. Effects of calcination temperature on physical parameters of mesoporous titania microspheres were studied by using X-ray diffraction (XRD), N_2 adsorption–desorption, Fourier transform infrared (FT-IR) spectra, high-resolution transmission electron microscope (HRTEM) and scanning electron microscopy (SEM). The photocatalytic activity of mesoporous titania spheres was also evaluated by photocatalytic degradation of phenol as a probe pollutant under UV irradiation. This work may provide a new insight into preparation of novel mesoporous titania spheres.

2. Experimental

2.1. Chemicals and materials

Titanium dioxide (P25) with purity of at least 99.5% was obtained from Degussa. A commercial anatase TiO_2 (a-TiO_2, purity >99.7%) was purchased from Xiamen Micaren Technology Co., Ltd. (Xiamen, China). Chitosan with 91% of deacetylation degree prepared from shrimp shell was purchased from Yuhuan Ocean Biochemical Co., Ltd. (Zhejiang, China). Titanium isporpoxide (reagent grade, 98%) was purchased from Aladdin Industrial Co., Ltd (Shanghai, China). Poly(vinyl alcohol) (98% hydrolyzed, average molecular weight 105,000) purchased from Shanghai Chemical Reagent Co. Ltd. (Shanghai, China) was of analytical reagent grade. Other chemical agents used were all analytical grade and all solutions were prepared with double distilled water.

2.2. Preparation of mesoporous titania spheres

A formation scheme of mesoporous titania spheres using chitosan/PVA hydrogel beads as a template is presented in Fig. 1. Firstly, chitosan/PVA hydrogel beads were prepared by an instantaneous gelation method [29]. Two grams of chitosan was dissolved into 50 mL of 5% (v/v) aqueous acetic acid to obtain a chitosan solution. Two grams of PVA was dissolved in 50 mL of double distilled water to form PVA aqueous solution under mechanical stirring at $70 \pm 1\,^{\circ}C$. Then, PVA solution was mixed homogenously with chitosan solution to form composite gel-forming mixture with vigorous stirring for 3.0 h at 30 °C. The resulting mixture was dropped into sodium hydroxide bath (500 mL, 0.5 M) through a 0.8 mm internal diameter syringe needle, forming chitosan/PVA hydrogel beads. The hydrogel beads were kept overnight in sodium hydroxide solution for complete solidifying, and then washed with double distilled water, ethanol and isopropyl alcohol to obtain swollen chitosan/PVA hydrogel beads, respectively.

Swollen chitosan/PVA hydrogel beads were soaked in the 98% titanium isopropoxide solution for 48 h at room temperature under closed conditions. Titanium isporpoxide molecules diffused slowly into swollen chitosan/PVA hydrogel matrix. Then, hydrogel beads with titanium isopropoxide were immersed into excess water for 24 h to cause the hydrolysis and condensation of titanium isopropoxide to take place in the chitosan/PVA polymer matrix. The resultant spheres were washed with double distilled water to remove titanium hydroxide deposited on the surface of these spheres. Finally, the spheres were dried in the oven at 60 °C till constant weight. Uncalinated titania spheres prepared in the above-described method were labeled as UTS. Following the drying process, the samples were calcined under 400, 500, 600, or 700 °C for 4 h in air at a heating rate of 1 °C/min, respectively. During calcination, the polymeric template was burnt off, and the inorganic precursor crystallized, forming inorganic spheres of mesoporous titania spheres [30]. Calcined titania spheres were labeled as CTS-400, CTS-500, CTS-600 and CTS-700 according to different calcination temperature, respectively.

2.3. Characterization

X-ray diffraction (XRD) patterns of the samples were recorded on a Rigaku diffractometer using Cu Kα irradiation (0.1540 nm) in an 2θ range of 5–75°. Thermogravimetric (TG) curves were performed on Model STA 409 PC Luxx at a heating rate of 10 °C/min. Nitrogen adsorption–desorption isotherms were carried out on a Micromeritics ASAP2020 apparatus at 77 K. Scanning electron microscopy (SEM) and high-resolution transmission electron microscopy (HRTEM) measurements were performed on a Hitachi S-4800 and JEOL JEM-2010, respectively. FT-IR spectra were measured at room temperature on a FT-IR-8400 spectrometer (Shimadzu, Japan).

2.4. Photocatalytic activity measurements

Photocatalytic experiments were carried out in a Pyrex-glass reactor (inner diameter: 29 mm and height: 9.1 mm), thermostated at 25 °C with a water jacket. An aqueous suspension (50 mL) containing 0.43 mM phenol and 1.0 g/L photocatalyst was first stirred in dark for 1 h to attain adsorption–desorption equilibrium and then irradiated with a high pressure mercury lamp (300 W, Shanghai Mengya) with a 320 nm cutoff filter. The distance between the reactor and the lamp was fixed at 10 cm. The light intensity reaching external surface of the reactor was 1.41 mW/cm^2, as measured by an UV-irradiance meter (UV-A, Instruments of Beijing Normal University, China). At given intervals, 2.5 mL of suspension was withdrawn by a microsyringe and filtered through a mephenolrane (0.22 μm in pore size). Organic substrates were analyzed by high-performance liquid chromatography (HPLC) on a Dionex P680 (Apollo C18 reverse column, and 50% CH_3OH aqueous solution as an eluent).

3. Results and discussion

3.1. Optical photographs

Fig. 2 displays typical optical photographs of chitosan/PVA hydrogel beads, UTS and CTS-500. Transparent chitosan/PVA hydrogel beads and white UTS are spherical with a diameter of ca. 3–4 mm as shown in Fig. 2a and b. Fig. 2c indicates that calcined titania spheres (UTS-500) have a little bit poor sphericity. At the same time, average out diameter of UTS-500 was decreased from 3–4 mm to 1.5–2 mm, which resulted from a shrinking from original size during calcination [19]. The result is in a good agreement with the fact that surface area and pore volume decreased significantly after calcination.

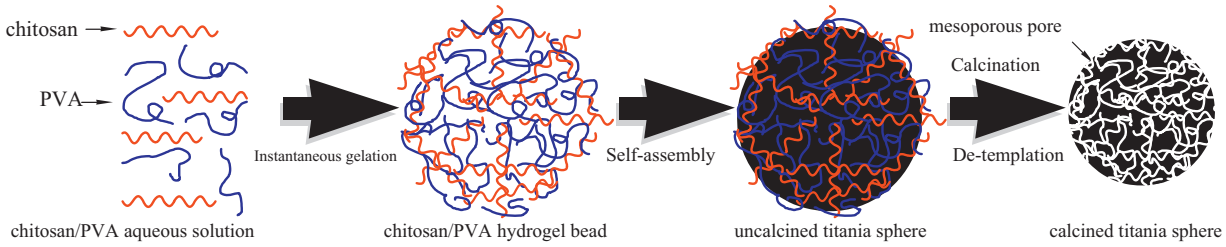

Fig. 1. A formation scheme of mesoporous titania spheres using chitosan/PVA hydrogel beads as template.

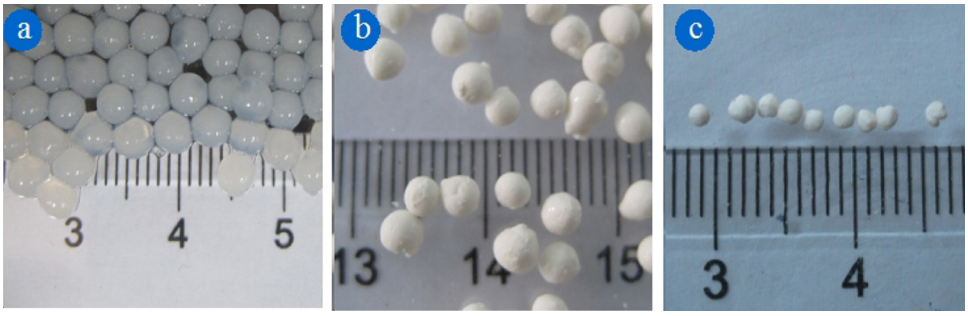

Fig. 2. Optical photographs of CS-PVA beads (a), UTS (b) and CTS-500 (c).

3.2. XRD analysis

Fig. 3 shows XRD patterns of as-synthesized UTS, CTS-400, CTS-500, CTS-600 and CTS-700. Uncalcined titania spheres (UTS) are nearly amorphous (Fig. 3a), which indicated that the as-dried precursor showed noncrystalline nature. When titanium isopropoxide is hydrolyzed at room temperature, the rate of hydrolysis reaction is relatively low and hydrolysis may be not complete. There was a great amount of un-hydrolyzed alkyls in UTS, which resulted in preventing phase transformation of amorphous to anatase [32]. Generally, XRD pattern of chitosan exhibited two broad diffraction peaks with different intensities at $2\theta = 10^\circ$ and 20° [33]. However, two characteristic peaks of chitosan disappeared in XRD pattern of as-synthesized UTS, which revealed that chitosan has some unordered existence in uncalcined titania spheres. In addition, due to its high content of amino and hydroxyl groups of chitosan in UTS, CS has also been combined with titanium in UST.

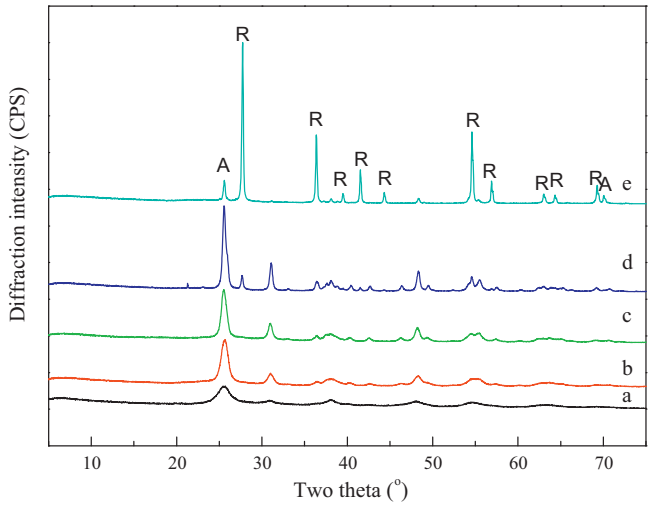

Fig. 3. XRD patterns of as-synthesized and calcined titania microspheres. (a) UTS, (b) CTS-400, (c) CTS-500, (d) CTS-600 and (e) CTS-700. The peaks marked A and R represents the anatase and rutile phase, respectively.

The CTS-400 and CTS-500 samples display characteristic peaks of anatase TiO_2 (JCPDS card No. 21-1272). With increasing calcination temperature (from 400 to 500 °C), the peak intensity of anatase increases and the width of (1 0 1) plane diffraction peak of anatase ($2\theta = 25.7^\circ$) become narrower, which indicated that the crystallization of mesoporous titania was enhanced [31]. Anatase crystallite size of calcined titania spheres was estimated by employing Debye–Scherrer equation. Average crystallize size of UTS-400 is about 5.4 nm, which is much smaller than that of CTS-500 (9.8 nm). Therefore, relative low-temperature is advantageous to maintain small crystallize size of TiO_2. When calcination temperature increases up further to 600 °C, CTS-600 contains both anatase and rutile phase. An additional phase of rutile was observed in CTS-600, indicating that anatase (A) begins to transform into rutile (R) at 600 °C. Almost complete transformation from anatase to rutile took place at 700 °C (CTS-700). According to some research, anatase phase is irreversibly converted to rutile phase in the range of 600–700 °C due to its lower thermal stability [34]. In addition, among three different forms of titania (anatase, rutile and brookite), anatase is the most photoactive form [34]. As a result, the photocatalytic activity of mesoporous titania spheres calcined at 500 °C (CTS-500) could be more effective than those calcined at other temperatures.

3.3. N_2 adsorption–desorption isotherms and porous nature

Fig. 4 shows nitrogen adsorption–desorption isotherms and Barrett–Joyner–Halenda (BJH) pore-size distribution plots of UTS and calcined titania spheres at different temperatures. Isotherms of calcined titania spheres exhibited the typical type IV adsorption isotherms, indicating the characteristics of mesoporous materials according to the IUPAC classification (Fig. 4a) [7]. With increase of calcined temperature, hysteresis loop shifted to higher relative pressure, indicating the loss of mesoporous structure at higher temperature. Except for as-synthesized samples (UTS), with increasing the calcined temperature from 400 to 700 °C, the surface area and pore volume decline significantly. The as-prepared sample showed a larger surface area of 233.56 m^2/g. While the sample was calcined at 400 and 500 °C for 4 h, it still presents a high specific surface area of 136 and 95 m^2/g (Table 1), respectively. CTS-700 exhibits

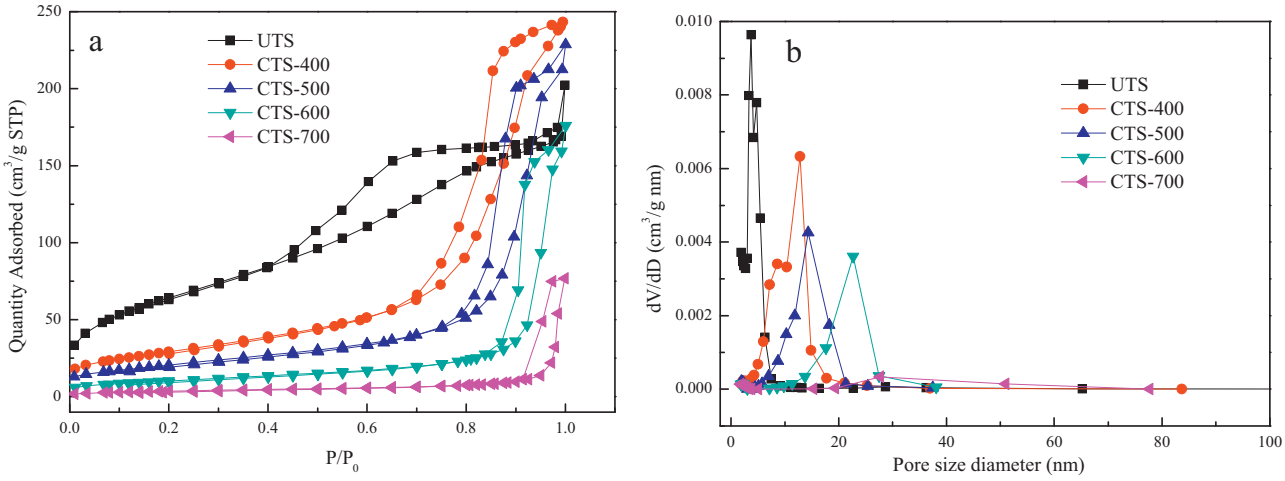

Fig. 4. N_2 adsorption–desorption isotherms (a) and pore size distribution curves (b) of (a) UTS, CTS-400, CTS-500, CTS-600 and (e) CTS-700.

a much lower surface area (13.39 m^2/g). As reported in literature, this is caused by a collapse of pore structure and an increase of particle size [18]. It is clear that corresponding pore volumes of CTS-400 and CTS-500 are greater than UTS, indicating that chitosan/PVA template was removed gradually from those materials. However, when calcination temperature increase further from 500 to 700 °C, pore volume of CTS decreased obviously from 0.354 to 0.119 cm^3/g. On the other hand, the crystalline size and the mean pore size of the samples increased gradually with an increase of calcination temperature. Pore size distribution curves indicate that the sample exhibit maxima at 4.74, 10.12 and 13.58 nm for UTS, CTS-300 °C and CTS-500, respectively (Fig. 4b). Pore-size distribution of TS-500 is narrow and centered at 13.58 nm, implying its well-defined mesoporous structure. Therefore, calcination temperature should be well at 500 °C unless the crystal size is controlled by other methods.

3.4. TEM and SEM

TEM images of as-synthesized CTS-400, CTS-500, CTS-600 and CTS-700 were illustrated in Fig. 5. Average particle sizes of CTS-400, CTS-500, CTS-600 and CTS-700 are approximately 9, 16, 19, 28 nm in size (Fig. 5a, b, d and e), respectively. Corresponding measured sizes from TEM image are in good agreement with the values determined by XRD analysis. Obviously, with increasing calcination temperatures, average crystallite size and average pore size increased, which indicated an enhancement of crystallite growth of mesoporous titania [18]. Further observation suggests that a large number of mesopores come from the aggregation of primary particles. Fig. 5c shows corresponding HRTEM image of CTS-500 sample. It shows clear lattice rings, indicating that CTS-500 was well crystalline. The fringes of 0.35 nm match that of (1 0 1) crystallographic plane of anatase TiO_2. According to Yu's model [32], nucleation of primary TiO_2 particles resulted from hydrolysis of titanium isopropoxide. Following nanocrystalline mesoporous anatase TiO_2 particles were formed by thermal crystallization. At the same time, organic framework in the samples was sintered partially and the crystallite size became larger with increasing calcination temperature (from 400 to 700 °C).

The mesostructure is also confirmed by SEM. Fig. 6 shows the SEM images of as-synthesized UTS (a1–a3), CTS-500(b1–b3) and CTS-700(c1–c3). The corresponding diameter of single dispersed spherical particle was in the following decreasing order: UTS (a1) < CTS-500(b1) < CTS-700(c1), indicating that there is a shrinking during calcination. SEM also proven further that average crystallite size increased with increasing calcination temperatures (a3 < b3 < c3). Then a thermal treatment converts the as-made amorphous TiO_2 into anatase TiO_2 and maintains original mesostructure. It is worthy that average crystallite size increased obviously with further increasing thermal temperature (from 500 to 700 °C). In fact, some studies have proven that both crystalline polymer fraction of PVA and the degradation and deacetylation of chitosan will occur when temperature is above about 500 °C [29]. It can be observed that pore channels are wormhole-like. Mechanism for developed porosity on film surface after adding TiO_2 in CS/PVA as a template is not well understood. Some studies explained these with the hypothesis as TiO_2 particles possibly holding CS molecules against centrifugal forces applied during the preparation process and calcinations [35]. The collapse of narrowest pores in CTS-700 is obvious. The result is in a good agreement with the fact that CTS-700 possesses poor sphericity and small pore volume.

3.5. FT-IR

FT-IR spectra of as-synthesized UTS, CTS-400, CTS-500, CTS-600 and CTS-700 are recorded and shown in Fig. 7. Before calcination, UTS has some obvious absorbency. There are some peak in a range of 3000–3400 cm^{-1} due to the combination of H–O–H of adsorbed water and –NH functional groups of chitosan in UTS (Fig. 7a) [36,37]. In addition, there exists a significant peak at 1078 cm^{-1} assigned to

Table 1
Structural properties of as-synthesized and calcined titania microspheres.

Sample	Calcination temperature (°C)	Average crystallize size (nm)	%Anatase	BET surface area (m^2/g)	Pore volume (cm^3/g)	Pore size diameter (nm)
UTS	As-synthesized	4.9	/	233.56	0.313	4.72
CTS-400	400	8.9	100	105.52	0.376	10.12
CTS-500	500	12.2	100	74.17	0.354	13.58
CTS-600	600	16.4	85	37.08	0.272	19.95
CTS-700	700	20.5	13	13.39	0.119	29.24

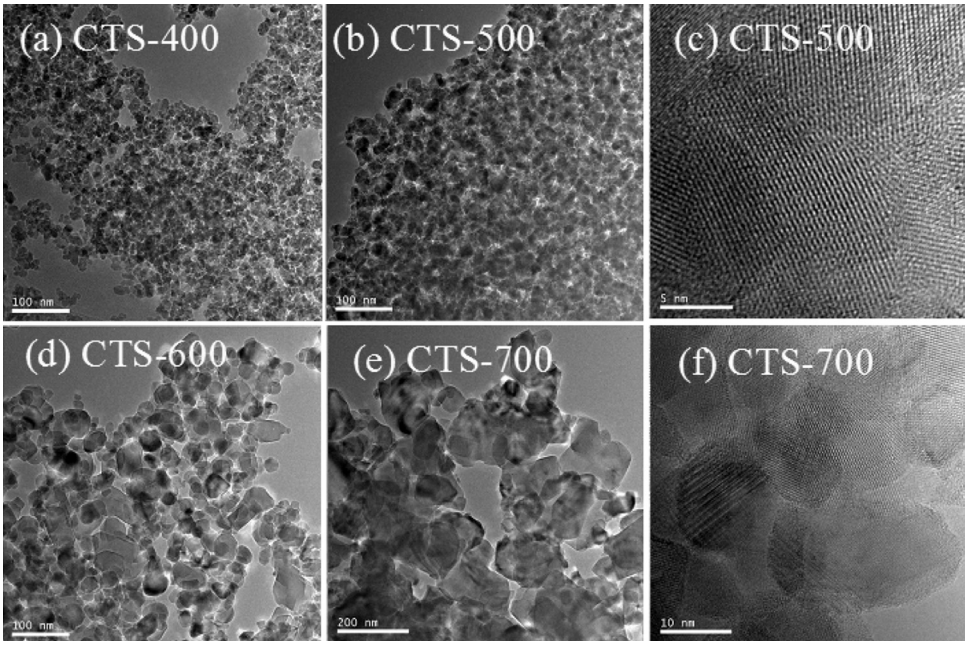

Fig. 5. The TEM patterns of samples: (a) CTS-400, (b and c), CTS-500, (d) CTS-600 and (e and f) CTS-700.

C–O vibrational stretching [26]. The absorption peak at 1629 cm^{-1} was assigned to N–H bending vibration in amine groups of chitosan [38]. In FT-IR spectrum of as-synthesized UTS, C–C stretching (1074 cm^{-1}) of PVA is also found [39]. After calcination, two absorption peaks at 1629 and 1074 cm^{-1} weakened and disappeared. Additionally, compared with FT-IR spectrum of uncalcined sample (Fig. 7a), the absorption peak at 3400 cm^{-1} disappeared in FT-IR spectra of calcined titania spheres. This phenomenon has proven that calcined titania spheres possess less surface hydroxyl content, which resulted from the fact that chitosan/PVA template was removed gradually from those materials. However, all calcined titania spheres display a strong absorption peak around 500 cm^{-1} attributed to Ti–O–Ti lattice vibrations [39], indicating that the crystallization of mesoporous titania appeared and was enhanced.

3.6. TG-DSC investigation

To determine calcined temperature at which chitosan/PVA template was removed and inorganic phase began to crystallized, thermogravimetric and differential thermal analysis was

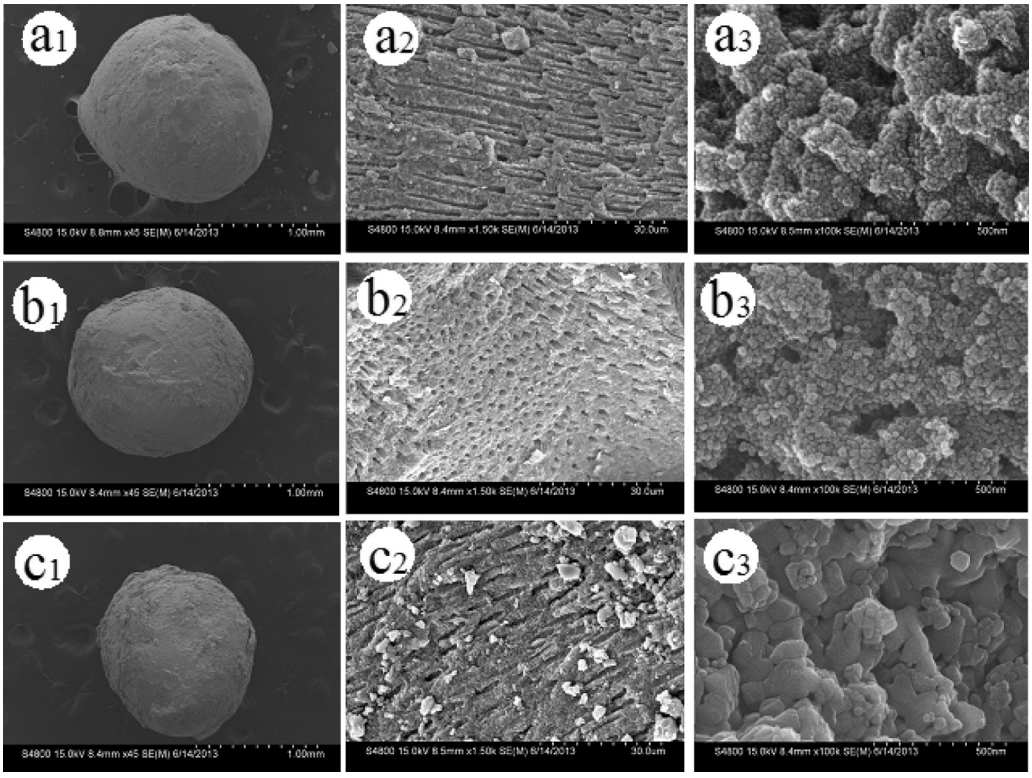

Fig. 6.

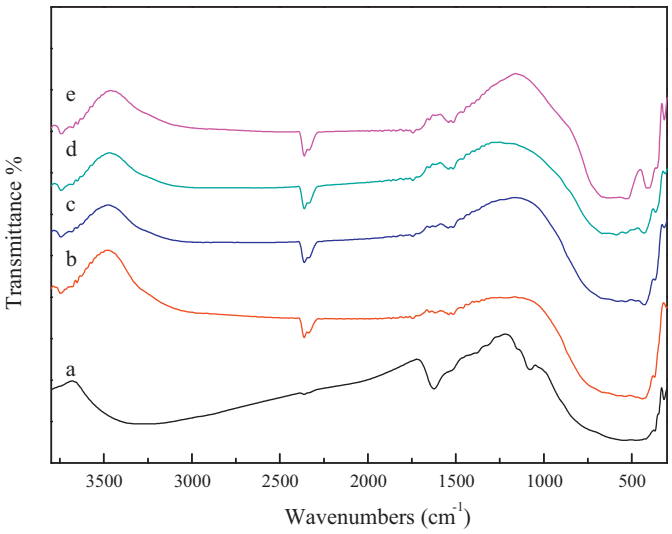

Fig. 7. FT-IR spectra of as-synthesized and calcined titania microspheres. (a) UTS, (b) CTS-400, (c) CTS-500, (d) CTS-600 and (e) CTS-700.

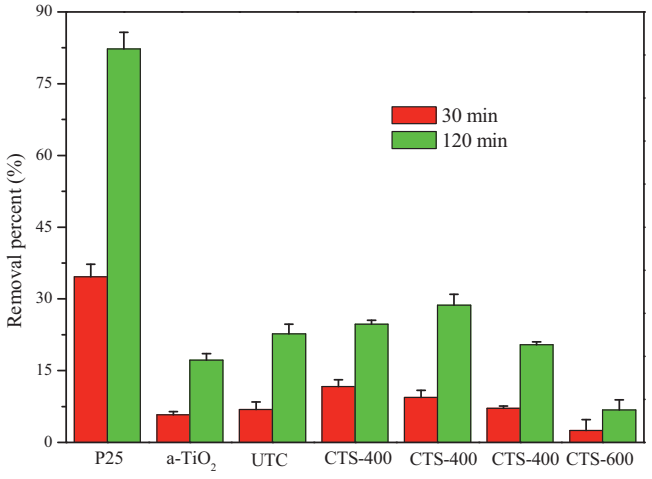

Fig. 9. Comparison of photocatalytic activities of uncalinated titania spheres, calcined titania spheres, P25 and a-TiO_2.

performed on the non-calcined sample in dynamic air atmosphere. TGA-DTA curves (Fig. 8) show that total weight loss was about 58.09% in three distinct regions. The first exothermic loss of 44.37% (up to 100 °C) is attributed to the loss of adsorbed and bound water and the residue of acetic acid [29,40]. Since chitosan contains –NH_2 and –OH functional groups, hydrogen bonding force is strongly formed among molecules [29]. The second endothermic loss of 13.55% in the temperature range from 100 to 400 °C is attributed to degradation of residual templated organics, i.e. chitosan and PVA [41]. In addition, high temperature above 200 °C leads to dehydrate condensation reaction between surface hydroxyl groups [42]. Finally, no further weight loss occured above 400 °C, indicating that a mesoporous titania sphere is formed successfully and all the chitosan/PVA template was removed from the materials. According to the fact that all calcined titania spheres were calcinated above temperature 400 °C, therefore organic templates (chitosan and PVA) have been removed during calcination.

3.7. Photocatalytic activity

The photocatalytic activities of uncalinated titania spheres, calcined titania spheres and commercial-grade TiO_2 are evaluated by photocatalytic removal of phenol used as a probe molecule under UV light irradiation. The results were presented in Fig. 9. As seen in Fig. 9, calcination temperature had an obvious effect on the photocatalytic removal of phenol from aqueous solution. Generally, there was no obvious photocatalytic activity in as-prepared TiO_2 powders consisted of an amorphous phase according to Yu's study [43,44]. However, in this study, removal of phenol still reached 23.2% by uncalinated titania spheres after 2 h under UV light irradiation. Chitosan is also known to bind dye molecules and could be used for dye adsorption since a large number of active amino (–NH_2) and hydroxyl (–OH) groups in chitosan chains can serve as coordination sites [15,29]. With an increase in calcination temperature from 400 to 500 °C, the removal of phenol increased from 24.7% to 28.7%. Upon further increasing calcination temperature to 600 and 700 °C, the removal of phenol decreased to 20.4% and 6.8%, respectively. Compared with other samples prepared in this study, CTS-500 displays a much higher photocatalytic removal efficiency of organic pollutants. The better photocatalytic performance of CTS-500 is attributed to its higher surface area and excellent crystallization of mesoporous titania. At first, both the specific surface area and pore volume of CTS-500 (74.17 and 13.58 m^3/g, respectively) are much higher than that of CTS-600 and CTS-700. What's more important, the peak intensities of anatase at CTS-600 increase and the width of the (1 0 1) plane diffraction peak of anatase ($2\theta = 25.7°$) becomes narrower. Some previous researches have indicated that anatase is the most photoactive form among the three forms of titania (anatase, rutile and brookite) [34]. Hydroxyl radicals (•OH) that have been deemed to be the major active species during the photocatalytic oxidation can be photogenerated effectively under UV light irradiation [45]. As a result, the photocatalytic activity of the mesoporous titania spheres calcined at 500 °C (CTS-500) is more effective than those calcined at other temperatures. For the convenience of comparison, two kinds of commercial TiO_2 i.e. Degussa P-25 TiO_2 (P25) and commercial anatase TiO_2 (a-TiO_2, purity >99.7%) were used to treat phenol solution under the same conditions. The removal efficiency of phenol by CTS-500 is calculated to be 28.7%, which is about third and 1.57 times of P25 (82.3%) and a-TiO_2, respectively. It is well known that P25 has excellent photocatalytic activity [44]. However, according to practical drawbacks of P25, such as agglomeration during utility and difficulty in separating and reclaiming them from treated effluent, CTS-500 is still a good alternative to treat organic pollutant in aqueous solution.

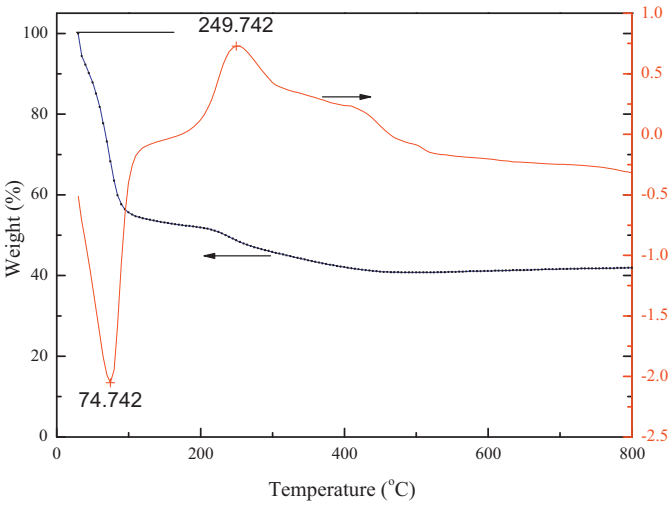

Fig. 8. TG-DSC curves of UTS.

4. Conclusions

Mesoporous titania spheres using chitosan and PVA hydrogel beads as template have been successfully synthesized. Nitrogen adsorption–desorption isotherm measurement, XRD, FT-IR, SEM and TEM have been used to characterize the mesoporous titania spheres. With increasing calcination temperature, the average crystallite size and average pore size increased while the Brunauer–Emmett–Teller (BET) specific surface areas, porosity and pore volumes steadily decreased. Results of characterization proved that prepared titania spheres were mesoporous structure. The photocatalytic activity of the mesoporous titania spheres calcined at 500 °C was more effective than those calcined at other temperatures, which were attributed to the porous structure, larger BET surface area, higher crystalline, and smaller crystallite size.

Acknowledgement

This work was supported by the Professional Development Foundation of a Visiting Scholar from Education Department of Zhejiang Province (Grant No. FX2012058), the Scientific and Technological Development Project of Taizhou City (Grant No. 121KY05) and the National Natural Science Foundation of China (Grant No. 21007044 and No. 51208331).

References

[1] Q.J. Xiang, J.G. Yu, M. Jaroniec, Graphene-based semiconductor photocatalysts, Chem. Soc. Rev. 41 (2012) 782–796.
[2] S. Morales-Torres, L.M. Pastrana-Martínez, J.L. Figueiredo, J.L. Faria, A.M.T. Silva, Design of grapheme-based TiO_2 photocatalysts—a review, Environ. Sci. Pollut. Res. 19 (2012) 3676–3687.
[3] R. Jiang, H.Y. Zhu, X.D. Li, L. Xiao, Visible light photocatalytic decolourization of C. I. Acid Red 66 by chitosan capped CdS composite nanoparticles, Chem. Eng. J. 152 (2009) 537–542.
[4] R. Jiang, J. Yao, H.Y. Zhu, Y.Q. Fu, Y.G. Guan, L. Xiao, G.M. Zeng, Effective decolorization of congo red in aqueous solution by adsorption and photocatalysis using novel magnetic alginate/γ–Fe_2O_3/CdS nanocomposite, Desalination Water Treat. 52 (2014) 238–247.
[5] U.G. Akpan, B.H. Hameed, Parameters affecting the photocatalytic degradation of dyes using TiO_2-based photocatalysts: a review, J. Hazard. Mater. 170 (2009) 520–529.
[6] W. Wang, C. Lu, Y. Ni, F. Peng, Z. Xu, Enhanced performance of {001} facets dominated mesoporous TiO_2 photocatalyst composed of high-reactive nanocrystals and mesoporous spheres, Appl. Surf. Sci. 265 (2013) 438–442.
[7] H. Hao, J. Zhang, Low temperature synthesis of crystalline mesoporous titania with high photocatalytic activity by post-treatment in nitric acid ethanol solution, Mater. Lett. 63 (2009) 106–108.
[8] A.H. Sun, Z.X. Li, M. Li, G.J. Xu, Y. Li, P. Cui, Room temperature synthesis of spherical mesoporous titania, Powder Technol. 201 (2010) 130–137.
[9] X.H. Yang, H.T. Fu, A.B. Yu, X.C. Jiang, Large-surface mesoporous TiO_2 nanoparticles: synthesis, growth and photocatalytic performance, J. Colloid Interface Sci. 387 (2012) 74–83.
[10] J. Hou, X. Yang, X. Lv, M. Huang, Q. Wang, J. Wang, Controlled synthesis of TiO_2 mesoporous microspheres via chemical vapor deposition, J. Alloys Compd. 511 (2012) 202–208.
[11] E.L. Crepaldi, G.J. de A.A. Soler-Illia, D. Grosso, F. Cagnol, F. Ribot, C. Sanchez, Controlled formation of highly organized mesoporous titania thin films: from mesostructured hybrids to mesoporous nanoanatase TiO_2, J. Am. Chem. Soc. 125 (2003) 9770–9786.
[12] E.Y. Kim, D.S. Kim, B.T. Ahn, Synthesis of mesoporous TiO_2 and its application to photocatalytic activation of methylene blue and *E. coli*, Bull. Korean Chem. Soc. 30 (2009) 193–196.
[13] Y. Jiang, Y. Luo, F. Zhang, L. Guo, L. Ni, Equilibrium and kinetic studies of C.I. Basic Blue 41 adsorption onto N, F-codoped flower-like TiO_2 microspheres, Appl. Surf. Sci. 273 (2013) 448–456.
[14] C. Dwivedi, V. Dutta, Size controlled synthesis and photocatalytic activity of anatase TiO_2 hollow microspheres, Appl. Surf. Sci. 258 (2012) 9584–9588.
[15] H.Y. Zhu, R. Jiang, Y.J. Guan, Y.Q. Fu, L. Xiao, G.M. Zeng, Effect of key operational factors on decolourization of methyl orange during H_2O_2 assisted nanosized CdS/TiO_2/polymer composite thin films under simulated solar light irradiation, Sep. Purif. Technol. 74 (2010) 187–194.
[16] M. Bidaoui, C. Especel, N. Bouchenafa-Saib, D. Duprez, O. Mohammedi, S. Royera, Citral hydrogenation on high surface area mesoporous TiO_2–SiO_2 supported Pt nanocomposites: effect of titanium loading and reduction temperature on the catalytic performances, Appl. Catal. A 445–446 (2012) 14–20.
[17] D.R. Sahu, L.Y. Hong, S.C. Wang, J.L. Huang, Synthesis, analysis and characterization of ordered mesoporous TiO_2/SBA–15 matrix: effect of calcination temperature, Microporous Mesoporous Mater. 117 (2009) 640–649.
[18] V. Loryuenyong, K. Angamnuaysiri, J. Sukcharoenpong, A. Suwannasri, Sol–gel derived mesoporous titania nanoparticles: effects of calcinations temperature and alcoholic solvent on the photocatalytic behavior, Ceram. Int. 38 (2012) 2233–2237.
[19] J. Choi, J. Kim, K.S. Yoo, T.G. Lee, Synthesis of mesoporous TiO_2/(–Al_2O_3 composite granules with different sol composition and calcination temperature, Powder Technol. 181 (2008) 83–88.
[20] H. Liu, Y.M. Du, J.H. Yang, H.Y. Zhu, Structural characterization and antimicrobial activity of chitosan/betaine derivative complex, Carbohydr. Polym. 55 (2004) 291–297.
[21] R. Jiang, H.Y. Zhu, J. Yao, Y.Q. Fu, Y.J. Guan, Chitosan hydrogel films as a template for mild synthesis of CdS quantum dots with highly efficient photocatalytic activity, Appl. Surf. Sci. 258 (2012) 3513–3518.
[22] A.N. Ozerin, A.N. Zelenetskii, T.A. Akopova, O.B. Pavlova-Verevkina, L.A. Ozerina, N.M. Surin, A.S. Kechek'yan, Nanocomposites based on modified chitosan and titanium oxide, Polym. Sci. 48 (2006) 638–643.
[23] Z. Zainal, L.K. Hui, M.Z. Hussein, A.H. Abdullah, I.R. Hamadneh, Characterization of TiO_2–chitosan/glass photocatalyst for the removal of a monoazo dye via photodegradation–adsorption process, J. Hazard. Mater. 164 (2009) 138–145.
[24] J.P. Jeun, Y.K. Jeon, Y.C. Nho, P.H. Kang, Effects of gamma irradiation on the thermal and mechanical properties of chitosan/PVA nanofibrous mats, J. Ind. Eng. Chem. 15 (2009) 430–433.
[25] J.M. Yang, W.Y. Su, T.L. Leu, M.C. Yang, Evaluation of chitosan/PVA blended hydrogel membranes, J. Membr. Sci. 236 (2004) 39–51.
[26] A.R. Fajardo, L.C. Lopes, A.F. Rubira, E.C. Muniz, Development and application of chitosan/poly(vinyl alcohol) films for removal and recovery of Pb(II), Chem. Eng. J. 183 (2012) 253–260.
[27] X. Li, Y. Li, Z. Ye, Preparation of macroporous bead adsorbents based on poly(vinyl alcohol)/chitosan and their adsorption properties for heavy metals from aqueous solution, Chem. Eng. J. 178 (2011) 60–68.
[28] E. Salehi, S.S. Madaeni, L. Rajabi, V. Vatanpour, A.A. Derakhshan, S. Zinadini, S. Ghorabi, H.A. Monfared, Novel chitosan/poly(vinyl) alcohol thin adsorptive membranes modified with amino functionalized multi-walled carbon nanotubes for Cu(II) removal from water: preparation, characterization, adsorption kinetics and thermodynamics, Sep. Purif. Technol. 89 (2012) 309–319.
[29] H.Y. Zhu, Y.Q. Fu, R. Jiang, J. Yao, L. Xiao, G.M. Zeng, Novel magnetic chitosan/poly (vinyl alcohol) hydrogel beads: preparation, characterization and application for adsorption of dye from aqueous solution, Bioresour. Technol. 105 (2012) 24–30.
[30] C. Dwivedi, N. Raje, J. Nuwad, M. Kumar, P.N. Bajaj, Synthesis and characterization of mesoporous titania microspheres and their applications, Chem. Eng. J. 193–194 (2012) 178–186.
[31] J.G. Yu, J.C. Yu, W.K. Ho, M.K.P. Leung, B. Cheng, G.K. Zhang, X.J. Zhao, Effects of alcohol content and calcination temperature on the textural properties of bimodally mesoporous titania, Appl. Catal. A 255 (2003) 309–320.
[32] J.G. Yu, G.H. Wang, B. Cheng, M.H. Zhou, Effects of hydrothermal temperature and time on the photocatalytic activity and microstructures of bimodal mesoporous TiO_2 powders, Appl. Catal. B 69 (2007) 171–180.
[33] J.S. Ahn., H.K. Choi., C.S. Cho, A novel mucoadhesive polymer prepared by template polymerization of acrylic acid in the presence of chitosan, Biomaterials 22 (2001) 923–928.
[34] P. Periyat, K.V. Baiju, P. Mukundan, P.K. Pillai, K.G.K. Warrier, High temperature stable mesoporous anatase TiO_2 photocatalyst achieved by silica addition, Appl. Catal. A 349 (2008) 13–19.
[35] R. Khan, M. Dhayal, Electrochemical studies of novel chitosan/TiO_2 bioactive electrode for biosensing application, Electrochem. Commun. 10 (2008) 263–267.
[36] K.M. Parida, N. Brundabana, Synthesis of mesoporous $TiO_{2-x}N_x$ spheres by template free homogeneous co-precipitation method and their photo-catalytic activity under visible light illumination, J. Colloid Interface Sci. 333 (2009) 269–276.
[37] C.H. Chen, F.Y. Wang, C.F. Mao, C.H. Yang, Studies of chitosan. I. Preparation and characterization of chitosan/poly(vinyl alcohol) blend films, J. Appl. Polym. Sci. 105 (2007) 1086–1092.
[38] C.E. Zubieta, P.V. Messina, C. Luengo, M. Dennehy, O. Pieroni, P.C. Schulz, Reactive dyes remotion by porous TiO_2-chitosan materials, J. Hazard. Mater. 152 (2008) 765–777.
[39] H.A. Shawky, Synthesis of ion-imprinting chitosan/PVA crosslinked membrane for selective removal of Ag(I), J. Appl. Polym. Sci. 114 (2009) 2608– 2615.
[40] S. Tripathi, G.K. Mehrotra, P.K. Dutta, Preparation and physicochemical evaluation of chitosan/poly(vinyl alcohol)/pectin ternary film for food-packaging applications, Carbohydr. Polym. 79 (2010) 711–716.
[41] D. Yang, J. Li, Z. Jiang, L. Lu, X. Chen, Chitosan/TiO_2 nanocomposite pervaporation membranes for ethanol dehydration, Chem. Eng. Sci. 64 (2009) 3130–3137.

[42] S. Chu, L. Luo, J. Yang, F. Kong, S. Luo, Y. Wang, Z. Zou, Low-temperature synthesis of mesoporous TiO_2 photocatalyst with self-cleaning strategy to remove organic templates, Appl. Surf. Sci. 258 (2012) 9664–9667.
[43] J. Yu, Y. Su, B. Cheng, Template-free fabrication and enhanced photocatalytic activity of hierarchical macro-/mesoporous titania, Adv. Funct. Mater. 17 (2007) 1984–1990.
[44] K. Lv, Q. Xiang, J. Yu, Effect of calcination temperature on morphology and photocatalytic activity of anatase TiO_2 nanosheets with exposed {0 0 1} facets, Appl. Catal. B 104 (2011) 275–281.
[45] Q. Xiang, J. Yu, P.K. Wong, Quantitative characterization of hydroxyl radicals produced by various photocatalysts, J. Colloid Interface Sci. 357 (2011) 163–167.